PARALLELIZED NUMERICAL CODE FOR DERIVATION OF HEAT TRANSFER COEFFICIENT FROM EXPERIMENTAL DATA

JANUSZ TELEGA, PIOTR DOERFFER,
RYSZARD SZWABA AND PIOTR KACZYŃSKI

The Szewalski Institute of Fluid-Flow Machinery, Polish Academy of Science
Fiszera 14, 80-231 Gdansk, Poland

(received: 23 January ; revised: 25 February 2015;
accepted: 27 February 2015; published online: 3 April 2015)

Abstract: An application of parallel computation capabilities in the MATLAB language for the analysis of experimental data concerning the heat transfer coefficient on ribbed walls is presented in this paper. A description of the experimental study, mathematical model and numerical implementation is also given. The obtained results of measurements and calculations shown here clearly indicate the influence of ribbed walls on the heat transfer coefficient distribution in an internal, subsonic flow.

Keywords: Matlab parallel computation, heat transfer coefficient, blade cooling

1. Introduction

During our measurements to examine the influence of various configurations of ribbed walls of the tunnel on the heat transfer phenomenon in internal subsonic flows it became clear that there was a need to develop an application for the analysis of experimental data which would allow derivating the heat transfer coefficient distribution.

2. Experimental stand

All the measurements were conducted using the experimental setup depicted in Figure 1.

Such an arrangement allows obtaining a stable flow of hot air in the test section. The mass flow rate is adjusted through the exchangeable nozzle (labelled as 'Orifice Plate' in Figure 1), working in maximum mass flow rate conditions.

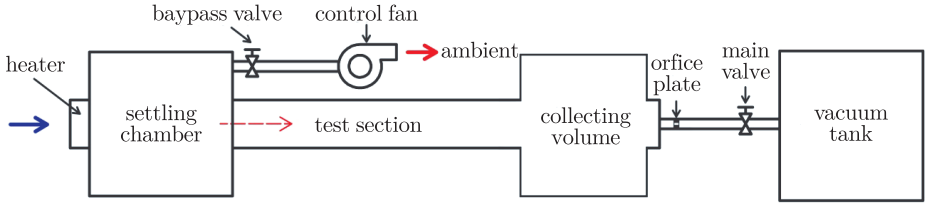

Figure 1. Scheme of the experimental stand

The section in which the measurement is taken is a tunnel of a rectangular cross-section, machined of transparent polycarbonate. Both the top and bottom walls of this section can be easily exchanged to allow testing of various rib configurations.

The visualization of the measurement section together with the orientation of the system of coordinates is shown in Figure 2.

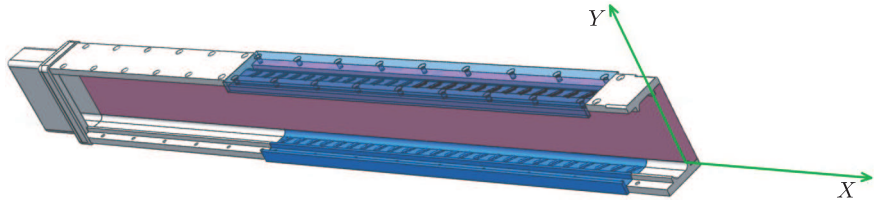

Figure 2. Visualization of the measurement section

The elements indicated in blue are the top and bottom walls and are interchangeable. In the actual experiments one set of smooth walls and two sets of walls with different ribbing were used. These elements and the back wall (Figure 2, brown) were covered with self-adhesive thermochromic liquid crystal foil (TLC foil) that changes its colour with the temperature).

The TLC colour evolution was recorded with a 3CCD-type camera and a system of two mirrors shown in Figure 3.

On the left-hand side of Figure 3, the scheme of the optical arrangement is presented, whereas the right-hand side depicts the image that can be recorded.

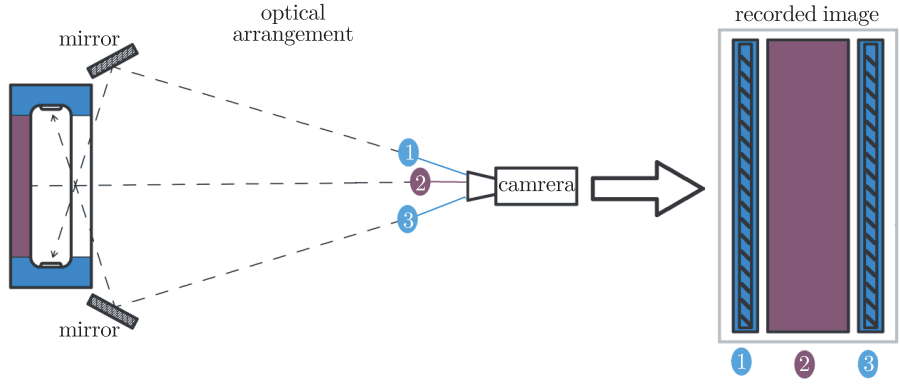

Figure 3. Optical arrangement of the recording system

The aim of introducing the mirrors to the system was to record results from the whole measurement area (bottom wall, back wall and top wall) in a single measurement, and thus having the data from the whole domain synchronized.

Additionally, thermocouples connected to a PC measurement card were applied in four points: at the inlet, the outlet and in two points equally spaced between them. One of the channels of this card was recording a logical signal form the controller of the main valve. The state of the valve was also indicated by a red LED diode, placed in the area visible for the camera.

An actual frame recorded during the measurement is shown in Figure 4. The figure also indicates the positions of thermocouples, the LED diode and the screws (non-transparent) indicated with white ellipses. The black surface on the back wall and between the ribs on the bottom wall and on the top wall is cold TLC foil.

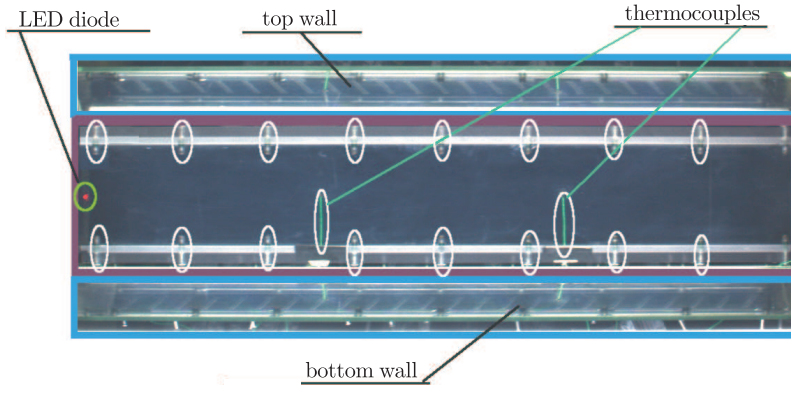

Figure 4. An actual frame recorded by the camera during the measurement

The complete set of measurement data resulted in a movie file (depicting the evolution of TLC colours at the walls, like in Figure 3) and a text file with a record of the temperatures and the state of the main valve. Due to technical reasons, first the ADC measurement was turned on, then the camera was switched on, and finally (after about 5 seconds) the flow of hot air could start. As a result of this, the raw data from the camera and PC voltage measurements were not synchronized.

3. Mathematical model ofthe phenomenon

For the analysis we used the solution of the equation of one dimensional heat transport for a semi-infinite plate with a step change of temperature [1]:

$$\frac{T_{w,\mathrm{LC}}(x,y,t)-T_i}{T_{f,\mathrm{aw}}(x,y)-T_i}=1-\exp\left(h^2(x,y)\frac{t}{k}\right)\cdot\mathrm{erfc}\left(h(x,y)\sqrt{\frac{t}{k}}\right) \tag{1}$$

with:

$T_{w,\mathrm{LC}}(x,y,t)$ – the temperature of the liquid crystal [K];
$T_{f,\mathrm{aw}}(x,y)$ – the temperature of the gas [K];

T_i – the initial temperature of the whole measurement section [K];
t – the time needed for reaching the $T_{w,\mathrm{LC}}(x,y,t)$ temperature [s];
$h(x,y)$ – the investigated heat transfer coefficient (HTC);
k – a constant describing the thermal properties of polycarbonate.

To reduce the complexity of calculations, the following assumptions concerning the parameters of the phenomena were made:

Temperature distribution evolution **($T_{w,\mathrm{LC}}(x,y,t)$)**

One constant value was chosen and fixed for the function. This value was adjusted to be adequate to the appearing of the maximum value of the green component in the TLC spectrum. This allowed reducing the computational cost by analysing only the green component (omitting the necessity of analysing the red and blue component reducing the computational time of this stage by 65%). On the basis of the calibration conducted for the TLC used for the measurement, this value was determined to be 35.1°C.

The distribution of gas temperature **($T_{f,\mathrm{aw}}(x,y)$)**

It was assumed that this distribution was a function of the X coordinate only, and it did not depend on the position in the direction normal to the flow which resulted in: $T_{f,\mathrm{aw}}(x,y) = T_{f,\mathrm{aw}}(x)$. The distribution of $T_{f,\mathrm{aw}}(x)$ was interpolated based on the thermocouple readings.

The above assumptions significantly reduce the complexity of Equation (1) to the following form:

$$\frac{T_{w,\mathrm{LC}} - T_i}{T_{f,\mathrm{aw}}(x) - T_i} = 1 - \exp\left(h^2(x,y)\frac{t_{\mathrm{LC}}(x,y)}{k}\right) \cdot \mathrm{erfc}\left(h(x,y)\sqrt{\frac{t_{\mathrm{LC}}(x,y)}{k}}\right) \qquad (2)$$

with $t_{\mathrm{LC}}(x,y)$ being the time of reaching the desired temperature at the point (x,y).

4. Numerical implementation

The program solving the investigated problem has been written in the MATLAB language. During the computation process, three main stages can be highlighted: data synchronization, determination of equation parameters and solving the equation using parallel computing.

The first stage synchronizes the data recorded by the camera with the thermocouple and valve readings. This is based on analysing the voltage from the valve controller and the camera frames. The application finds the moment of valve opening in the text file and in the movie material (the moment of opening of the valve can be determined concluding from the dynamics of the red component content in the frames). The preceding values of temperature readings and movie frames are discarded. The first non-rejected data set is assumed to be the beginning of the phenomenon and is assumed to be recorded at the time $t = 0\,\mathrm{s}$.

The second stage consists of calculations of the distributions of parameters using Equation (2). Taking advantage of the simplified assumption concerning

$T_{w,\mathrm{LC}}$, the determination of the $t_{\mathrm{LC}}(x,y)$ distribution is reduced to calculating the positions of maxima of the set of one variable functions, each describing the evolution of the value of the green component at every point of the frame, $G_{i,j}(t)$.

The scheme of obtaining the $G_{i,j}(t)$ function is depicted in Figure 5.

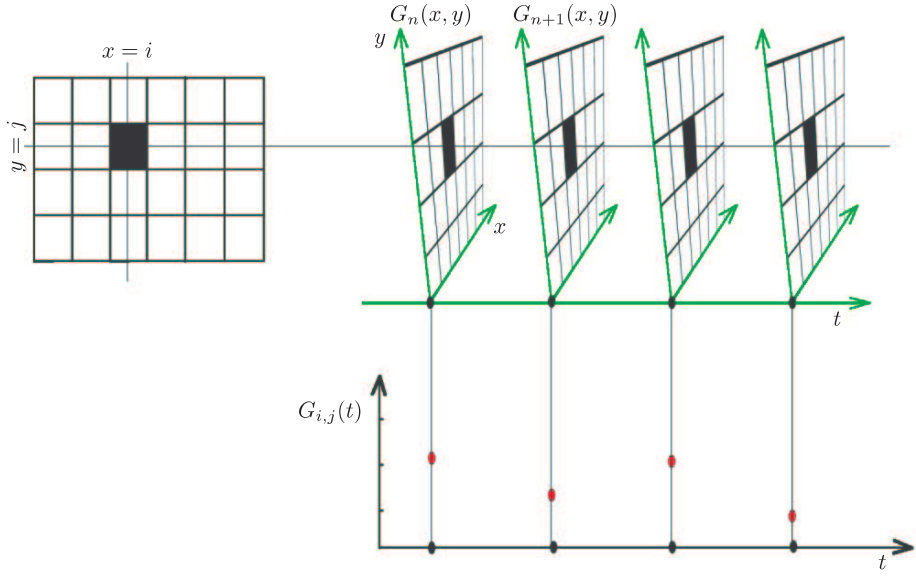

Figure 5. Determination of $G_{i,j}(t)$ function values

The left-hand side of the figure represents a selected point in the recorded image. The values of the green component in this point, recorded in subsequent frames, are taken to be the values of the $G_{i,j}(t)$ function for the moments of recording of these frames.

The $G_{i,j}(t)$ function is calculated at every point of the image (the resolution of the camera is 1200×1024, the time of the experiment is approximately 60s, and the number of frames per second is 30). This results in the three-index matrix of all the values of all the $G_{i,j}(t)$ functions, consisting of 10^9 elements. As the camera records every component (R,G,B) as a 8-bit value, thus the abovementioned matrix variable size is 10^9 bytes. A PC desktop computer used for the analysis was not capable of completing this numerically simple task. In order to overcome this issue, the domain is divided into a user-defined number of sub-regions. Calculations can be conducted for a domain divided into 100 parts. The results obtained from all the sub-regions are then combined into a complete $t_{\mathrm{LC}}(x,y)$ distribution.

4.1. Derivation of HTC

The form of Equation (2) indicates that there are no couplings between equations describing the domain points. Therefore, the derivation of the HTC distribution can be simplified to solving the same equation in each point of

the image, with correct values of parameters. Each of these equations can be solved independently. Taking this into account, this task is very well-suited for straightforward parallelization.

The MATLAB has a built-in parallel version of the 'for' loop. It is parallel in terms of dividing the control variable range and assigning the sub-ranges to the selected number of locally available CPU cores. This implementation has some limitations: neither can it be nested, nor is there any control over the assignment of the ranges of control variable values to the cores or control over the order of iteration execution (the order of execution of iterations **is not** in accordance with the ascending order of the control variable value).

In the considered case (Equation (2)), the only significant drawback that has to be taken in account is the lack of nested loops. To avoid a very natural approach for a two dimensional problem involving nesting of two loops (one for each dimension), all the matrices of parameters (of the size corresponding to the image size: 1200×1024 were reshaped to vectors ($1200 \cdot 1024$ in length).

Once the parameters are prepared in the vector form, Equation (2) can be solved in a (parallelized) loop with just one control variable. When all the CPU cores have completed the calculations, the resultant vector ($1200 \cdot 1024$) is reshaped back to the 1200×1024 matrix being directly relevant to the image.

Due to the repetitiveness of many settings, the application saves all the user-defined parameters (like temperatures, region of interest, input files localization output file localization) in a file. These files can be interpreted and used as 'starting scripts' for automated analysis.

5. Results

The distribution of $t_{\mathrm{LC}}(x,y)$ on the back wall, obtained from the same measurement as the exemplary frame in Figure 4, is shown in Figure 6.

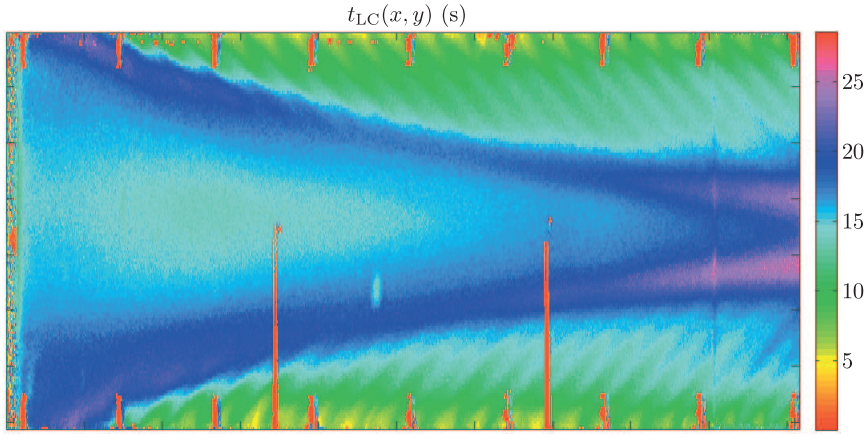

Figure 6. Distribution of $t_{\mathrm{LC}}(x,y)$ on the back wall (the time of reaching the desired temperature)

The image contains some dark blue zones without data. These correspond to the non-transparent elements within the image, like screws and thermocouples (marked by white ellipses in Figure 4). These elements shade the TLC, making it invisible to the camera.

Figure 7 depicts the distribution of HTC corresponding to the distribution of $t_{\mathrm{LC}}(x,y)$ from Figure 6.

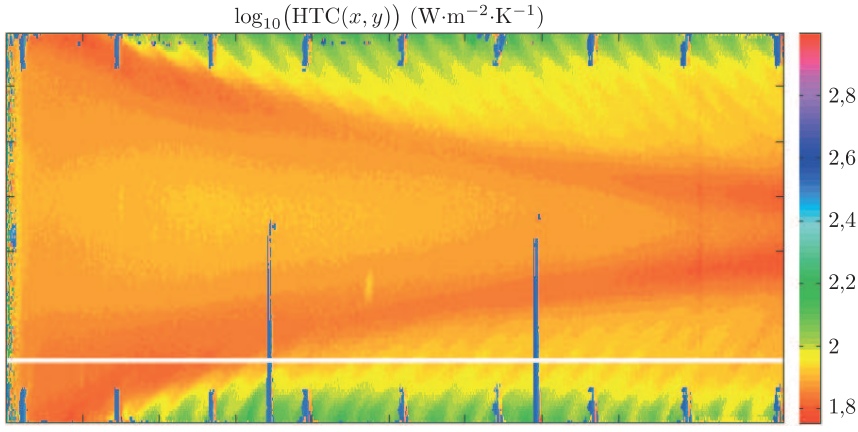

Figure 7. Distribution of $h(x,y)$ (heat transfer coefficient) on the back wall

Except for the separated non-transparent regions, the obtained distribution of the heat transfer coefficient reflects the nature of the phenomenon very well, with the main flow and periodic structures originating from the ribs on the walls clearly visible.

6. Post processing

Due to the colour resolution (8 bits) the obtained values of HTC are also quantified. The white horizontal line in Figure 7 indicates the position of taking the values for the distribution of HTC, depicted in Figure 8.

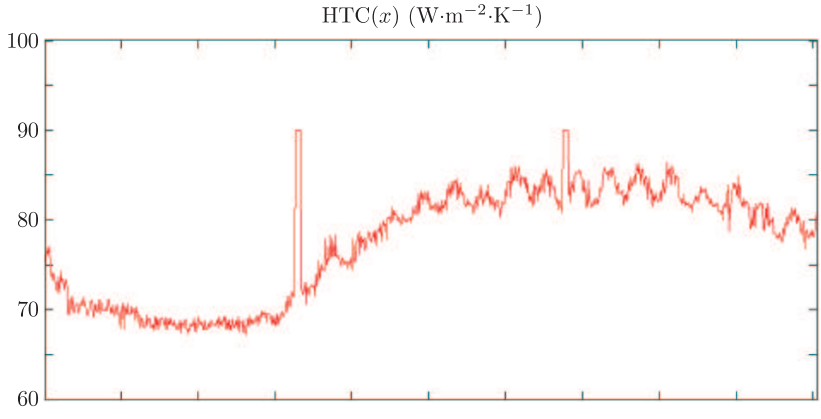

Figure 8. Distribution of HTC results along a selected line

The distribution in Figure 8 clearly indicates the presence of noise and quantization errors. As an attempt to diminish these problems, a 2-D low pass filter was applied. The resultant distribution of filtered data along the same line (marked in white in Figure 7) is depicted in Figure 9.

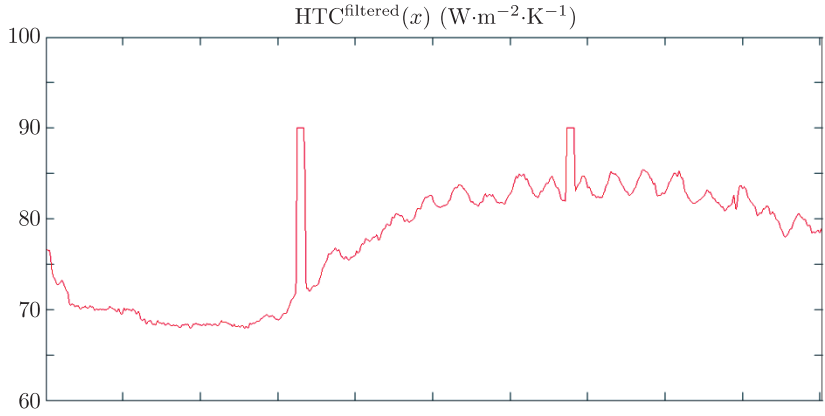

Figure 9. Distribution of filtered HTC results along a selected line

The filtered data is very clearly less noisy. A more physically significant result of filtering is shown in Figure 10. The bottom part of the figure contains a coloured contour plot of HTC (with only seven value ranges adjusted in a way to clearly show the region of strong influence of the ribbed wall). The top part of the figure depicts the distribution of the same values after application of the filter.

The top distribution suits the real distribution significantly better than the bottom one. The influence of the noise and finite resolution of the camera

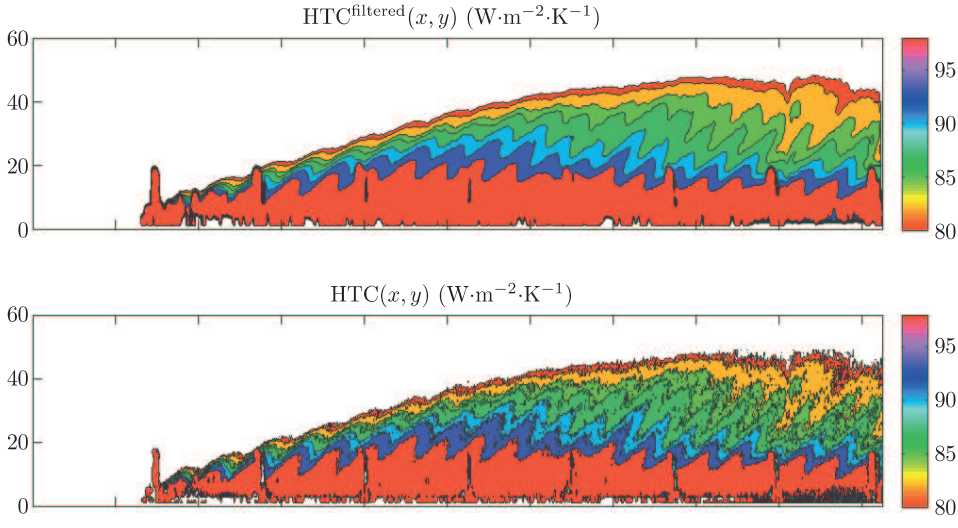

Figure 10. Comparison of measured (bottom) and filtered (top) fields of HTC

transducer has been diminished, while the spatially variable structure of the flow is well represented.

7. Conclusion

Taking the advantage of the nature of the phenomenon and some assumptions on the mathematical model, it was possible to parallelize the code in a very straightforward manner and thus take the benefit of the full computational potential of the system. In this way, satisfying parameters of parallel calculations were achieved. Figure 11 presents the dependence of the speed-up on the size of the computational domain (left plot) and on the number of the CPU core (right).

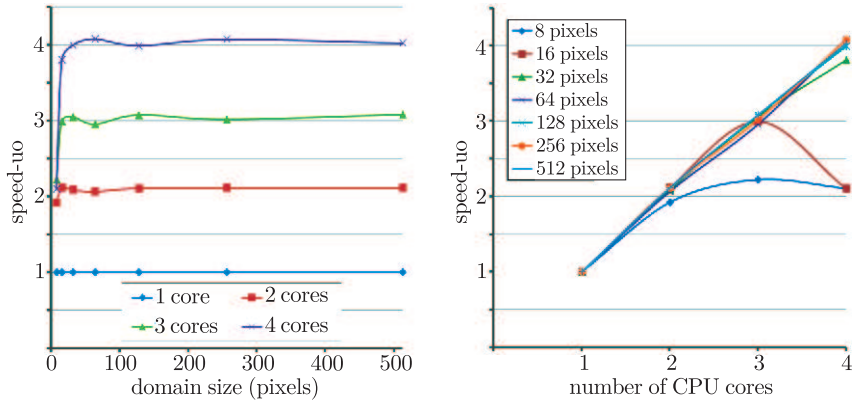

Figure 11. Speed-up as a function of computational domain size (left) and as a function of the number of CPU cores (right)

The size of the domain in the plots is given in the number of pixels being the square root of the size of the computational domain (the domain is a square, whereas the graph is plotted as a function of the length of its side). The distributions indicate a satisfying (linear) speed-up for a reasonably large domain size (larger than 32×32 pixels).

As the resolution of the applied CCD camera is only 1 Megapixel, it was possible to analyze the results of the present experiment on a desktop-class computer. In future experiments it is planned to obtain data of a significantly higher resolution (either by using a high resolution digital camera or by using an analogue camera and later digitizing the recorded images). Once this is accomplished, the code can be run in a high-performance computational centre, fully exploiting the computational resources.

References

[1] Vogel G, Graf A B A, Wolfersdorf von J, Weigand B 2003 *Transactions of the ASME* **125**